BBA - Molecular Basis of Disease 1871 (2025) 167705

Contents lists available at ScienceDirect

BBA - Molecular Basis of Disease

journal homepage: www.elsevier.com/locate/bbadis

Exogenous hydrogen sulfide and NOX2 inhibition mitigate ferroptosis in pressure-induced retinal ganglion cell damage

Yuan Feng, Xiaosha Wang, Panpan Li, Xin Shi, Verena Prokosch, Hanhan Liu *

Department of Ophthalmology, Faculty of Medicine and University Hospital of Cologne, University of Cologne, 50937 Cologne, Germany

ARTICLE INFO

Keywords:
Retinal ganglion cells
iron metabolism
Mitochondrial function
Ferroptosis
Hydrogen sulfide
glaucoma therapy

ABSTRACT

Glaucoma, a leading cause of irreversible blindness worldwide, is characterized by the progressive degeneration of retinal ganglion cells (RGCs). While elevated intraocular pressure (IOP) significantly contributes to disease progression, managing IOP alone does not completely halt it. The mechanisms underlying RGCs loss in glaucoma remain unclear, but ferroptosis—an iron-dependent form of oxidative cell death—has been implicated, particularly in IOP-induced RGCs loss. There is an urgent need for neuroprotective treatments. Our previous research showed that hydrogen sulfide (H_2S) protects RGCs against glaucomatous injury. This study aims to investigate the interplay between elevated pressure, mitochondrial dysfunction, iron homeostasis, and ferroptosis in RGCs death, focusing on how H_2S may mitigate pressure-induced ferroptosis and protect RGCs. We demonstrate alterations in iron metabolism and mitochondrial function in a subacute IOP elevation model in vivo. In vitro, we confirm that elevated pressure, iron overload, and mitochondrial dysfunction lead to RGCs loss, increased retinal ferrous iron and total iron content, and heightened reactive oxygen species (ROS). Notably, pressure increases NADPH oxidase 2 (NOX2) and decreases glutathione peroxidase 4 (GPX4), a key regulator of ferroptosis. NOX2 deletion or inhibition by H_2S prevents pressure-induced RGCs loss and ferroptosis. Our findings reveal that H_2S chelates iron, regulates iron metabolism, reduces oxidative stress, and mitigates ferroptosis, positioning slow-releasing H_2S donors are positioning as a promising multi-target therapy for glaucoma, with NOX2 emerging as a key regulator of ferroptosis.

1. Introduction

Glaucoma is one of the most prominent causes of irreversible vision loss [1]. It is a disease marked by damaging optic nerve and loss of visual function, typically resulting from irreversible damage and death of retinal ganglion cells (RGCs). While elevated intraocular pressure (IOP) serves as the primary risk factor and the primary factor linked to glaucoma progression [2,3], solely managing IOP does not fully impede disease advancement [4,5]. Even under treatment, some patients experience blindness in at least one eye for a follow-up period of 15 to 20 years [6–8].

Certainly, beyond elevated IOP, various other pathogenic factors contribute to RGCs loss. Identifying and managing these causal factors are essential for controlling and improving glaucoma prognosis. The underlying mechanisms are still unclear and neuroprotective treatments are an unmet need.

Hydrogen sulfide (H_2S) is identified as an innovative endogenous gaseous signaling molecule [9]. Being a strong reducing agent, H_2S is vital in various pathological and physiological processes, including reducing inflammation, mitigating oxidative stress, and restoring energy balance [10–13]. H_2S exhibits significant therapeutic potential in various neurodegenerative diseases within the central nervous system [14–17]. In recent years, more and more studies have centered on the connection between H_2S and glaucoma.

Alterations in endogenous H_2S levels in the retina have been associated with different pathological conditions. Exogenous H_2S donors have demonstrated the potential to protect RGCs against various insults [18–20]. In a previous study, we observed alterations in a glaucoma model with endogenous H_2S synthase. Additionally, a slow-release H_2S donor GYY4137 [morpholin-4-ium 4 methoxyphenyl(morpholino) phosphinodithioate] was effective in protecting RGCs from glaucomatous damage [21]. H_2S's neuroprotective effects are attributed to inducing vasodilation, mitigating oxidative stress, regulating nerve endocrine function, and suppressing inflammation [22–24], but the precise mechanisms involved are still not fully understood.

Our previous study revealed that acute IOP elevation disrupts iron

* Corresponding author.
E-mail address: hanhan.liu@uk-koeln.de (H. Liu).

https://doi.org/10.1016/j.bbadis.2025.167705
Received 10 June 2024; Received in revised form 17 January 2025; Accepted 30 January 2025
Available online 4 February 2025

regulation in the retina [25], consistent with findings from other studies that also reported interference with iron metabolism in RGCs in acute IOP elevation models [26]. Iron is essential for retinal function and metabolism [27]. Yet, excessive iron accumulation in neural tissue is considered to be critical in cortical and retinal diseases [28]. Epidemiological studies have shown a positive connection between a high iron intake, elevated serum ferritin levels, and an increased risk of glaucoma [29–31]. Iron homeostasis is crucial for the optic nerve and RGCs, suggesting targeted therapies focusing on iron regulation could be effective. Iron-induced retinal damage often results from mitochondrial dysfunction, excessive generation of reactive oxygen species (ROS), and neuroinflammatory responses [32–34]. In contrast, the specific role of iron in glaucoma pathogenesis and retinal neurodegeneration requires further investigation. The discovery of ferroptosis provides a novel framing for understanding glaucoma pathogenesis through the lens of iron metabolism [35].

Ferroptosis, triggered by disruptions in glutathione peroxidase activity, leads to reduced antioxidant capacity and increased lipid ROS, ultimately causing oxidative cell death [36,37]. The process has been linked to glaucoma and is identified as a promising target for glaucoma treatment [26,38]. Our earlier research demonstrated pathways involved in iron regulation, mitochondrial homeostasis, and ROS scavenging are activated by exogenous H_2S, which plays a crucial role in preventing ferroptosis [25]. Nonetheless, H_2S can chelate iron, as its (S^{2-}) ion binds freely with radical iron, exerting protective effects against neural iron overload [39], a promising therapeutic approach for neurodegenerative diseases.

The intricate interplay between elevated pressure, mitochondrial dysfunction, H_2S, and ferroptosis remains underexplored. To unravel the roles of ferroptosis and H_2S in the context of pressure induced RGCs loss, it is important to determine (a) the susceptibility of RGCs to iron accumulation, (b) alterations in retinal iron content and regulation due to elevated mechanical stress leading to ferroptosis, (c) the cellular signals and events are involved and (d) the potential therapeutic implications of H_2S in mitigating ferroptosis.

2. Result

2.1. Significant alterations in retinal protein abundance following subacute intraocular pressure elevation: implications for iron metabolism and mitochondrial function

The proteomics analysis yielded the identification of 5754 proteins, and subacute IOP elevation (IOP group) led to a significantly reduced abundance of 54 proteins and an increased abundance of 506 proteins (Fig. 1A).

According to the PANTHER gene classification analysis, 21 proteins were classified as mitochondrial proteins and/or related to iron metabolism (Supplementary Table1), 12 proteins were significantly more abundant in response to subacute IOP elevation, and 9 proteins whose abundance was significantly reduced (Supplementary Table1). The five most significantly up-regulated proteins were Hemopexin (*Hpx*), 39S ribosomal protein L17, mitochondrial (*Mrpl17*), Galectin-3 (*Lgals3*), Methionine-R-sulfoxide reductase B2, mitochondrial (*Msrb2*), and Coiled-coil domain-containing protein 115 (*Ccdc115*) (Fig. 1B). The five most significantly down-regulated proteins were NADH dehydrogenase [ubiquinone] iron-sulfur protein 4, mitochondrial (*Ndufs4*), NADH dehydrogenase [ubiquinone] flavoprotein 1, mitochondrial (*Ndufv1*), MICOS complex subunit Mic60(*Immt*), DnaJ homolog subfamily C member 11(*Dnajc11*), and Microsomal glutathione S-transferase 3 (*Mgst3*) (Fig. 1C).

2.2. Pathway analysis of retinal differentially expressed proteins associated with iron metabolism and mitochondrial function

To determine whether specific pathways related to iron metabolism and mitochondrial function were regulated differently under subacute IOP elevation, analyses using the Kyoto Encyclopedia of Genes and Genomes (KEGG) and Gene Ontology (GO) were conducted.

According to GO analysis, biological processes in the form of regulation of translation, protein transport, aerobic respiration, and mitochondrial ATP synthesis coupled proton transport were mostly affected by subacute IOP elevation (Fig. 1D). The changes in cellular components were most significant in macromolecular complex, respiratory chain, and mitochondrial respiratory chain complex I (Fig. 1E). In molecular function, macromolecular complex binding, protein kinase binding, NADH dehydrogenase (ubiquinone) activity, among others were significantly changed following subacute IOP elevation, especially "metal ion binding" which involves 118 genes (Fig. 1F). KEGG pathway analysis indicates that three pathways with the most significant fold enrichment (FE) metrics were ferroptosis (FE = 4.2257), chemical carcinogenesis - reactive oxygen species (FE = 3.8069), and parkinson's disease (FE = 3.5214). Meanwhile, the pathway with the most proteins enriched was Pathways of neurodegeneration - multiple diseases, with 37 relevant proteins being enriched (Fig. 1G).

Protein-protein interaction networks between the selected proteins were generated based on known interactions using STRING analysis (Fig. 1H). The three networks showed a high concentration of proteins involved in iron homeostasis, ferroptosis, and glutathione metabolism. Furthermore, proteins involved in oxidative phosphorylation were enriched and interacted with *Gpx4* from the ferroptosis and iron homeostasis (Fig. 1H).

2.3. Iron overload, pressure, mitochondrial mutations, and H_2S protection on RGCs survival

We investigated the effects of iron toxicity, high pressure, and mitochondrial mutation on RGCs. Both excess iron (1316 ± 182.0 RGC/mm^2) and elevated pressure (1233 ± 222.8 RGC/mm^2) resulted in significantly reduced RGCs survival compared with controls (1549 ± 238.0 RGC/mm^2) ($P < 0.0001$). Hemin concentration is determined by a pilot experiment, 500 nM led to similar RGCs loss compared to 60 mmHg. The survival of RGCs from retinal explants cultured with H_2S precursors (1479 ± 154.1 RGC/mm^2) showed a marked increase relative to the pressure group ($P < 0.0001$). No significant difference was observed when compared to the control group (1549 ± 238.0 RGC/mm^2) (Fig. 2A, B).

The number of RGCs was significantly reduced in mtDNA mutator (2104 ± 290.7 RGC/mm^2) compared with WT mice (3060 ± 304.2 RGC/mm^2) ($P < 0.0001$) (Fig. 2C, D). There are 31.24 % less RGCs in aged mtDNA mutator.

2.4. Iron accumulation in retina and brain

The iron content and composition were analyzed in the retinas subjected to iron overload and elevated hydrostatic pressure, as well as in the brains of mtDNA mutators. In retinal tissues cultured in vitro, both iron overload and elevated pressure resulted in increased total iron content and ferrous iron in retina. Total iron content and ferrous iron decreased significantly upon the addition of H_2S precursors ($p < 0.05$) (Fig. 3A). The percentage of ferrous iron in the total iron increased under iron overload (94.5 %) and elevated pressure (91.41 %) ($p < 0.0001$). Whereas, after being treated with H_2S precursor, the percentage of ferrous iron (89.97 %) was almost the same as that of the control (89.62 %) ($p > 0.05$) (Fig. 3B).

In the brain of mtDNA mutators, total iron content ($p < 0.0001$), and ferrous iron levels ($p < 0.01$) were substantially greater than their age-matched wild-type controls (Fig. 3C). And the percentage of ferrous iron (73.18 %) in brains of mtDNA mutator mice was lower compared to wild-type mice (85.9 %) ($p < 0.0001$) (Fig. 3D).

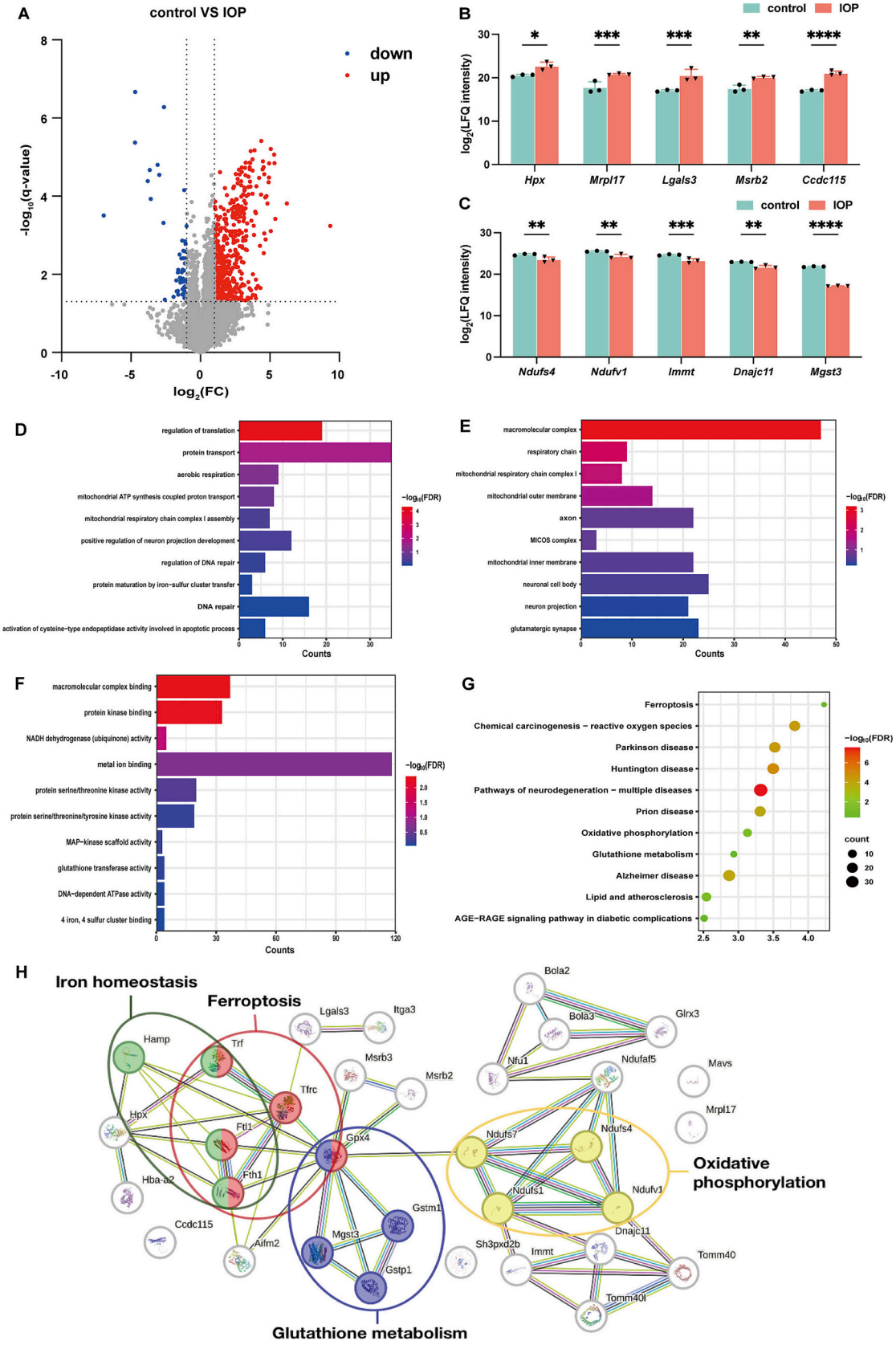

(caption on next page)

Fig. 1. Elevated intraocular pressure affects gene expression related to iron homeostasis and mitochondrial function in the retina.
(A) The volcano plot shows all differentially expressed proteins between the subacute IOP elevation group (IOP group) and the controls. The X-axis displays the log2 fold change in LFQ intensity between the compared groups, while the Y-axis represents − 1× log10 of the p-value for each protein. Red dots represent the proteins whose abundance increased under IOP elevation, blue dots represent those less abundant proteins and gray ones represent the proteins that are not significantly altered. (B) Some of the significantly up-regulated proteins, (C) and some of the significantly down-regulated proteins associated with mitochondrial and/or iron metabolism in the IOP group (n = 3 per group). (D-F) GO enrichment analysis bar plot for proteins with differential expression between the IOP and control groups. The X-axis denotes the quantity of genes that are enriched. The Y-axis denotes various GO terms. The bar represents −1× log10 of FDR. (G) The bubble plot shows KEGG enrichment analysis for proteins with differential expression between the IOP and control groups. The X-axis shows the ratio of differentially expressed proteins to total proteins in each pathway, while the dot color and size indicate the significance and extent of gene enrichment. (H) STRING analysis of proteins with altered expression linked to iron metabolism and mitochondrial function. Data are shown as mean ± SD; * $p < 0.05$, ** $p < 0.01$, *** $p < 0.001$, **** $p < 0.0001$ (using t-tests to compare with the control group). IOP: intraocular pressure, GO: Gene Ontology, KEGG: Kyoto Encyclopedia of Genes and Genomes, LFQ: label-free quantification, FDR: false discovery rate.

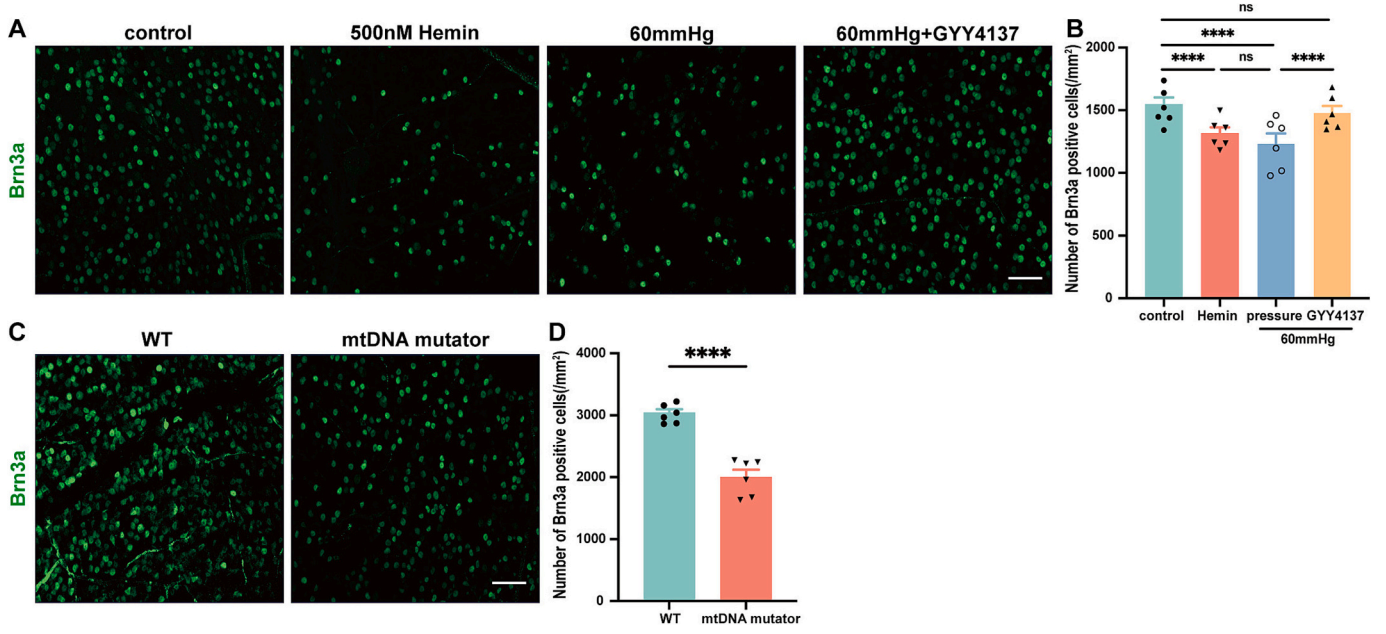

Fig. 2. Factors leading to RGCs death and the protective effect of H_2S.
(A, C) Representative fluorescence micrographs of Brn3a staining ($n = 6$ per group); (B, D) Statistical analysis of Brn3a-positive cell counts in the retina flat-mount (n = 6 per group). Data are shown as mean ± SD. **** $p < 0.0001$ (compared with the control group using one-way ANOVA and compared with WT group using *t*-tests). Scale bar = 50 μm. ns: no significance,

2.5. Iron dysregulation in retina under overload and elevated pressure

To investigate how elevated pressure affected iron homeostasis, we evaluated the localization and expression of four iron regulatory proteins in different layers of the retinas.

The transferrin receptor (TfR) binds extracellular non-heme iron and transferrin complexes, transferring iron into the cell via receptor-mediated endocytosis [40]. Immunochemical historical staining in the retinal cross-sections confirmed the expression of TfR throughout all retina layers, with emphasis on the ganglion cell layer (GCL), inner plexiform layer (IPL), and inner nuclear layer (INL) (Fig. 3E). Both iron overload and elevated pressure resulted in a dramatic increase in TfR fluorescence intensity in retina ($p < 0.0001$), particularly pronounced in retina inner layers ($p < 0.0001$). The fluorescence intensity of TfR decreased significantly when treated with H_2S precursor despite high-pressure exposure($p < 0.0001$) (Fig. 3F).

Hepcidin binds and degrades ferroportin, hindering iron export from cells and thereby limiting iron utilization and storage [41]. Our results showed that hepcidin is expressed throughout all layers of the retinas (Fig. 3E). Elevated pressure dramatically increased the fluorescence intensity of hepcidin in retina ($p < 0.0001$), especially in the GCL and the whole inner retina ($p < 0.0001$). However, no significant changes were observed in iron overload. Hepcidin fluorescence intensity decreased significantly when treated with H_2S precursor ($p < 0.0001$), showing no substantial difference from the control group, the change is particularly pronounced in the inner retina ($p < 0.0001$) (Fig. 3G).

To investigate the impact of high pressure on the stable intracellular iron, the localization and expression of the ferritins were analyzed. The Ferritins are responsible for storing iron in a stabilized form within cells [40]. Both ferritin heavy chains (FTH1) and ferritin light chains (FTL) were analyzed. Like other iron regulatory proteins, FTH1 and FTL were expressed across all retinal layers (Fig. 3E). The fluorescence intensity of FTH1 in the retina can be observed to be stronger in the pressure group (Fig. 3E), yet there is no significant difference in either iron overload group or pressure group comparing to control. H_2S precursor significantly reduced pressure-induced changes in FTH1 ($p < 0.0001$) (Fig. 3H). No notable difference is observed between the control and H_2S-treated group (Fig. 3H). Following high-pressure exposure, fluorescence intensity of FTL was not significantly changed in retina, nor in the GCL or the inner layer (Fig. 3I).

2.6. Elevated pressure-induced ROS and NOX2 activation in retina: H_2S protection

Ferrous iron is recognized as a potent oxidant, contributing to heightened oxidative stress within cells [42]. To investigate whether the increased total iron content and ferrous iron in the retina lead to increased oxidative stress, we measured ROS levels with DHE

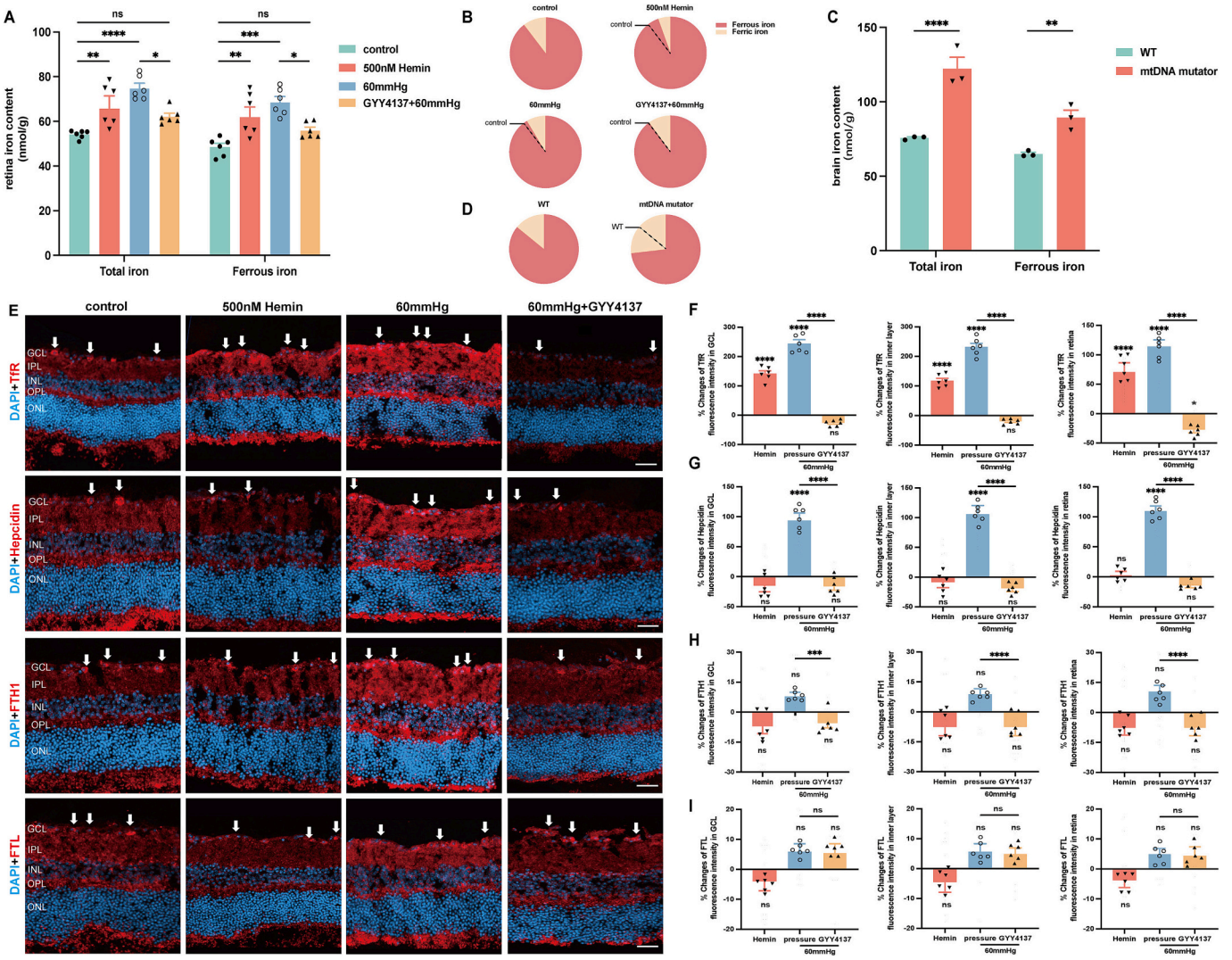

Fig. 3. Elevated hydrostatic pressure results in disturbed iron metabolism while H_2S effectively maintains iron homeostasis.
(A) Quantification of total iron and ferrous iron content in the retina cultured under iron overload and elevated hydrostatic pressure with or without H_2S precursor in vitro ($n = 6$ per group). (B) Iron composition in the retina; (C) Quantification of total iron and ferrous iron content in the brain of mtDNA mutators and WT group ($n = 3$ per group). (D) Iron composition in the brain of mtDNA mutators and the controls. (E) Representative fluorescence microscopy of TfR, Hepcidin, FTH1, and FTL staining with DAPI in retinal cryosections. The white arrows point to RGCs which exhibit higher fluorescence intensity compared to their surrounding tissue. (F-I) Changes in fluorescence intensity of TfR, Hepcidin, FTH1, and FTL in GCL, the inner retina, and the whole retina (n = 6 per group). Data are shown as mean ± SD. * $p < 0.05$, ** $p < 0.01$, *** $p < 0.001$, **** $p < 0.0001$ (compared with the control group using one-way ANOVA and compared with WT group using *t*-tests). Scale bar = 50 μm. ns: no significance, TfR: transferrin receptor, FTH1: ferritin heavy chains, FTL: ferritin light chains, GCL: ganglion cell layer.

(Dihydroethidium) assay. Iron overload increased the fluorescence intensity of DHE in the GCL compared with controls ($p < 0.01$), while the change in the inner retina and whole retina is not significant. Elevated pressure increased the fluorescence intensity of DHE in the whole retina ($p < 0.001$) (Fig. 4B-D). The changes were notably more emphasized in the inner retinal layers, especially in the GCL ($p < 0.0001$) (Fig. 4B, C). Nevertheless, H_2S reversed the pressure-induced increase of DHE fluorescence intensity in the retina, particularly in the GCL ($p < 0.0001$) (Fig. 4B, C).

One of the main functions of the NOX2 NADPH oxidase is to produce antimicrobial ROS [43]. The fluorescence intensity of NOX2 is not changed in the iron overload group, neither in the GCL nor the whole retina. Elevated hydrostatic pressure led to significantly stronger fluorescence intensity in GCL, the inner retina as well as the whole retina ($p < 0.0001$) (Fig. 4F-H). The introduction of H_2S precursor resulted in a substantial decrease in pressure-induced NOX2 fluorescence intensity ($p < 0.0001$) (Fig. 4F-H).

2.7. Pressure-induced ferroptosis in retina: H_2S restores antioxidant defense and Gpx4

Ferroptosis is a well-established pattern of regulated cell death marked by a deficiency in glutathione peroxidase 4 (Gpx4) activity and elevated ferrous iron levels, leading to cell death through membrane lipid peroxidation [44]. Glutathione (GSH) and Gpx4 are the cornerstones of the antioxidant defense.

To investigate whether the antioxidant defense of the retina is changed under iron overload and high pressure, we measured GSH levels in the retina. Both iron overload and elevated pressure significantly decreased GSH levels in retina ($p < 0.0001$) (Fig. 5A). GSH level could be restored by H_2S precursors, and there is no statistical difference between the control (17.39 ± 2.68 nmol/mg) and H_2S group (14.76 ± 1.52 nmol/mg) (Fig. 5A). GSH levels were notably lower in the brain of mtDNA mutator mice (68.27 ± 5.59 nmol/mg) compared to the wild-type controls (83.00 ± 5.37 nmol/mg) ($p < 0.05$, Fig. 5B).

The activity of the Gpx4 is also a core regulator of ferroptosis. While

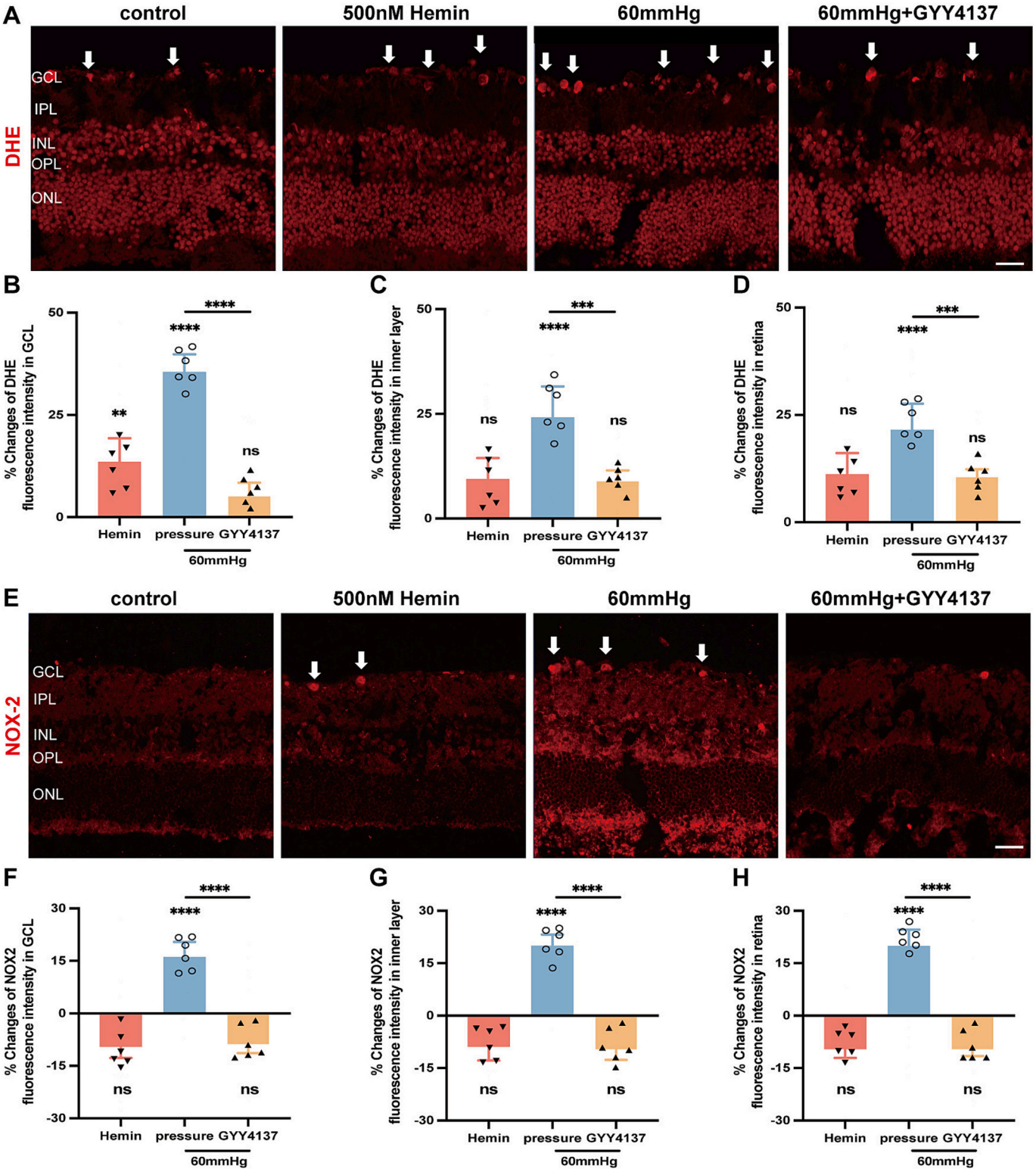

Fig. 4. Elevated hydrostatic pressure increased oxidative stress in the retina, and H_2S played an antioxidant role.
(A, E) Representative fluorescence micrographs of DHE and NOX2 staining in retinal cryo-sections The white arrows point to RGCs which exhibit higher fluorescence intensity compared to their surrounding tissue; (B-D, F-H) Changes in fluorescence intensity of DHE and NOX2 in GCL, inner layer, and the whole retina ($n = 6$ per group). Data are shown as mean ± SD. ns: no significance, ** $p < 0.01$, *** $p < 0.001$, **** $p < 0.0001$ (comparisons are analyzed using one-way ANOVA). Scale bar = 50 μm. DHE: dihydroethidium, GCL: ganglion cell layer.

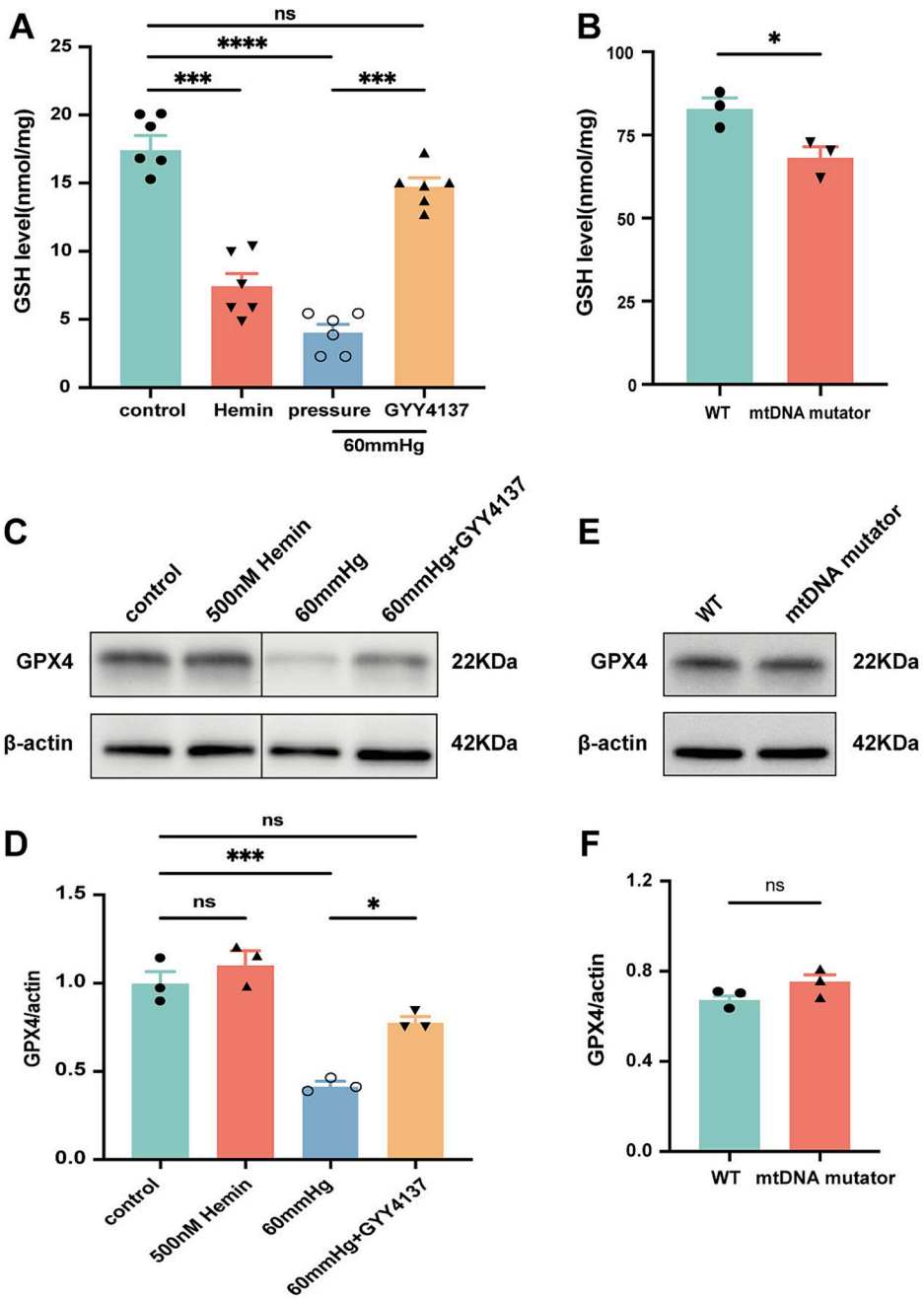

Fig. 5. H_2S effectively attenuated high-pressure-induced retinal ferroptosis.
(A, B) Quantification of GSH levels in retina ($n = 6$ per group) and in WT and mtDNA mutator mice brains ($n = 3$ per group). (C, D) The signal intensity of Gpx4 is significantly reduced in the retina subjected to elevated hydrostatic pressure, which is restored with H_2S precursor. Iron overload does not affect Gpx4 ($n = 3$ per group). (E, F) No difference in the signal intensity of Gpx4 is observed in brain tissue from mtDNA mutator mice and WT control. (n = 3 per group). Data are shown as mean ± SD. ns: no significance; * $p < 0.05$; *** $p < 0.001$; **** $p < 0.0001$(analyzed using one-way ANOVA for comparisons with the control group and *t*-tests for comparisons with WT).

iron overload and mitochondrial mutation showed no effect on Gpx4 expression in the retina and brain, elevated hydrostatic pressure significantly reduced the expression of Gpx4 in the retina, which can be restored by H_2S precursor (Fig. 5C-F).

2.8. *Elevated hydrostatic pressure did not inhibit Gpx4 activity in NOX2$^{-/-}$ mice*

Our previous study demonstrated that NOX2 deficiency mitigates glaucoma associated RGCs loss and neurodegeneration induced by elevated intraocular pressure [45]. To further elucidate the relationship between ferroptosis and NOX2, we investigated alterations in retinal Gpx4 expression under elevated pressure in NOX2$^{-/-}$ mice.

In NOX2$^{-/-}$ mice, the signal intensity of Gpx4 was not affected in the retina when subjected to subacute elevated intraocular pressure, as shown in Fig. 6.

3. Discussion

Studying the mechanisms underlying glaucoma development is a key research focus in ophthalmology [26,38,46]. The findings of this study provide new perspectives on the underlying mechanisms of glaucoma

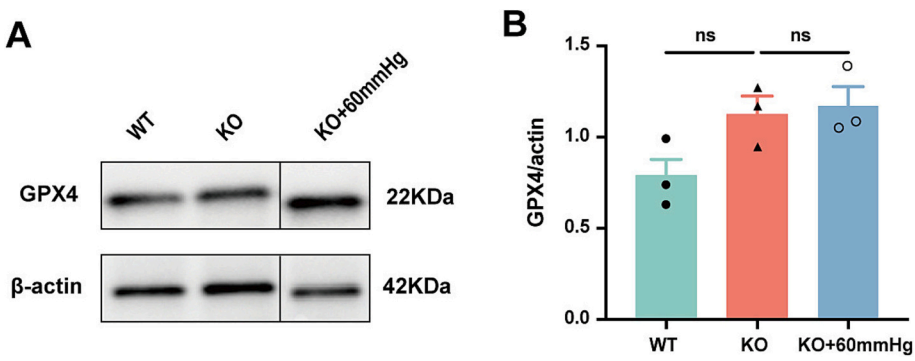

Fig. 6. Elevated hydrostatic pressure did not inhibit Gpx4 activity in NOX2$^{-/-}$ mice.
(A) Western blotting detection of Gpx4 level in WT and NOX2$^{-/-}$ mice retinas with or without pressure. (B) Gpx4 is notably higher in NOX2$^{-/-}$ mice retinas compared to WT, elevated pressure does not inhibit the Gpx4 level in retina of NOX2$^{-/-}$ mice (n = 3 per group). Data are shown as mean ± SD. ns: no significance (comparisons are analyzed using one-way ANOVA).

and the therapeutic implications of H_2S in mitigating ferroptosis.

Here, we illustrate how iron overload, mitochondrial dysfunction, and ferroptosis contribute to pressure-induced RGCs loss in subacute retinal injuries. NOX2 serves as a critical mediator of ferroptosis in the retina following elevated pressure. By inhibiting NOX2 with H_2S or knocking out NOX2, we can largely prevent RGCs death in experimental glaucoma. The neurotoxic effects of iron and ferroptosis in glaucoma, coupled with findings from other studies linking iron and ferroptosis concerning neurodegenerative disorders like Parkinson's, Alzheimer's, and Huntington's diseases, suggest that ferroptosis may be a common feature in the complex and varied responses of the central nervous system to prolonged injury [46–49].

We found that subacute elevated IOP led to alterations in pathways associated with iron homeostasis, mitochondrial dysfunction, and antioxidant defense, mirroring changes observed in our previous study with acute IOP elevation [25]. These findings are further supported by proteomic analyses of aqueous humor and serum samples from patients with primary angle-closure glaucoma, which also show similar disruptions in these pathways [31,50].

Under physiological conditions, iron levels in the retina are tightly regulated [37]. Excessive iron can lead to cytotoxic effects, while insufficient iron levels may result in cellular dysfunction [51]. Our experiments unveiled the susceptibility of RGCs to iron overload, characterized by elevated levels of total iron and ferrous iron. While both pressure injury and mitochondrial dysfunction led to increased total iron and ferrous iron levels in the tissue, pressure injury specifically increased the percentage of ferrous iron in the retina, and mitochondrial dysfunction led to reduced ferrous iron in the brain.

To identify potential contributors to abnormal iron metabolism following pressure-induced RGCs loss, we examined the three key factors regulating iron metabolism: iron import, export, and storage. Non-heme iron in the blood binds to transferrin and is internalized into cells via the transferrin receptor (TfR) on the retinal cell membrane [40,52]. Our findings revealed that elevated hydrostatic pressure increased TfR expression in the retina, indicating enhanced iron import capacity. Hepcidin, a crucial hormone for iron homeostasis, binds to and degrades ferroportin (Fpn), thereby limiting cellular iron export [40,53]. We found that pressure led to increased expression of hepcidin in the retina, which inhibited retinal iron export. Ferritin, composed of ferritin heavy chain (FTH) and ferritin light chain (FTL), is the primary iron storage protein [54]. Our study found that the expression of FTH and FTL remained largely unchanged following pressure injury, which corroborates the finding of increased retinal iron levels. Interestingly, the absence of notable alterations in iron storage proteins suggests that previously sequestered iron in ferritin was mobilized into the cytoplasm, leading to elevated levels of free ferrous iron in the retina.

Iron accumulation is a prevalent characteristic of numerous neurodegenerative diseases [55]. Our study revealed an elevation in both total iron levels and free ferrous iron in the retina following pressure injury. Ferrous iron is a strong oxidant that generates hydroxyl radicals through the Fenton reaction and Haber-Weiss reaction [42]. These radicals can oxidize lipid metabolites, particularly polyunsaturated fatty acids, resulting in the formation of cytotoxic lipid peroxides [56]. These are consistent with our findings that both pressure injury and iron overload led to increased ROS (DHE-derived fluorescence) and decreased GSH content in the retina. However, the involvement of iron in neurodegeneration encompasses more complexities than just oxidative damage.

Ferroptosis is an iron-driven cell death process marked by notable accumulation of ferrous iron and extensive lipid peroxidation [35,42]. Our previous study found that NOX2 deficiency can rescue glaucoma-related RGCs loss and neurodegeneration induced by elevated intraocular pressure [45]. Our findings align with this, as we observed high-pressure-induced ferrous iron accumulation and elevated ROS levels. Research has indicated that factors inducing ferroptosis can impact Gpx4, a glutathione peroxidase, leading to reduced antioxidant defenses and increased lipid ROS accumulation within cells, ultimately resulting in oxidative cell death [35,57–59]. Ferroptosis occurs when the level of lethal lipid peroxides exceeds the scavenging capacity of Gpx4 [59]. Whilst our study found that both excessive iron and mitochondrial dysfunction reduced GSH content, only pressure injury resulted in decreased Gpx4 expression. This suggests that ferrous iron accumulation and mitochondrial dysfunction reduce antioxidant capacity but are insufficient on their own to trigger ferroptosis. Instead, there appears to be an additional upstream factor activated by pressure that initiates ferroptosis.

Iron accumulation characteristic of ferroptosis can also collaborate with enzymes that generate ROS, such as NADPH oxidases (NOXs), leading to enhanced intracellular ROS production [36,60]. Our study showed increased NOX2 expression in the retina following pressure injury, while iron overload did not affect its expression. These results suggest a link between NOX2 and ferroptosis, and NOX2 may act as a primary initiator of pressure-induced ferroptosis, as evidenced by unchanged Gpx4 expression in NOX2 knockout mice under pressure injury.

In our earlier research, we observed a rise in endogenous H_2S synthases within a glaucoma animal model following sustained elevated IOP [21]. Moreover, H_2S donor markedly enhanced RGCs survival across various glaucomatous insults [21]. We subsequently found that H_2S exerts neuroprotective effects by targeting pathways disrupted by acute IOP elevation, including iron regulation, mitochondrial homeostasis, and retinal vascular function [25]. In the current study, we demonstrated that H_2S prevents pressure-induced RGCs loss by functioning as an iron chelator, binding to and effectively sequestering ferrous iron [61,62]. Notably, as a physiological gas transmitter, H_2S

possesses neuroprotective properties that extend beyond its chemical characteristics [63,64]. Our results revealed that H_2S influences iron regulatory proteins, reducing total iron content despite pressure injury. By chelating radical ferrous iron, H_2S contributed to restoring GSH contents and reduced ROS generation. Furthermore, H_2S also protects against pressure-induced ferroptosis by inhibiting NOX2.

A variety of pathological pathways contribute to the development of glaucoma. Our study emphasizes that disruptions in iron homeostasis, mitochondrial dysfunction, and impaired antioxidant defense significantly affect pressure-induced RGCs damage. Following pressure injury, total iron content, radical ferrous iron, and NOX2 levels increase in the retina, resulting in elevated ROS, decreased antioxidant capacity, and ferroptosis. While iron accumulation and mitochondrial dysfunction are central to ferroptosis, they alone are insufficient to trigger the process; heightened NOX2 activity plays a crucial role. Knockdown and pharmacological inhibition of NOX2 effectively reduced pressure-induced ferroptosis, diminished ROS generation, and improved RGCs survival. H_2S stabilizes iron homeostasis, chelates excess ferrous iron, and inhibits NOX2, thereby mitigating RGCs ferroptosis and protecting RGCs from pressure-induced damage (Fig. 7).

Elevated IOP leads to changes in mitochondrial function and iron metabolism. High pressure reduced iron export and increased iron import, while iron storage proteins were not affected. Coupled with the finding of increased retinal iron content following pressure injury, this suggests that the retinal ferrous iron content is increased. Increased iron content resulted in the generation of ROS. Both increased iron content and mitochondrial dysfunction led to reduced antioxidant capacity but not ferroptosis. Ferroptosis occurs primarily when NOX2 activity is heightened. H_2S can chelate free radical iron and reduce ferrous iron levels. It also influences iron regulatory proteins, resulting in a reduction in total iron content despite pressure injury. This, coupled with the chelation of radical ferrous iron, contributed to a restoration of GSH contents and reduced generation of ROS. Furthermore, H_2S also exerts its protective property by inhibiting NOX2 which subsequently protects RGCs from pressure-induced ferroptosis.

Even though subacute IOP elevation was effectively simulated using both in vivo and in vitro glaucoma mouse models, the mouse model cannot fully replicate the complex human environment. Additionally, some experiments had limited sample sizes due to objective constraints, which may restrict the generalizability of the results. While our study delved into the causes of pressure-induced retinal iron metabolism abnormalities and the protective mechanisms of H_2S, the complete mechanisms underlying iron metabolism dysregulation and the prolonged impact of interventions like H_2S still require further exploration. Meanwhile, H_2S's potential side effects and long-term safety have not been fully evaluated. Future studies are needed to further determine the optimal dosage, administration methods, and treatment duration of H_2S, as well as to investigate its effects on systemic pathways and signaling mechanisms to ensure its efficacy and safety in glaucoma treatment.

Our study is the first to explore the complex interplay between elevated pressure, mitochondrial dysfunction, iron homeostasis, and ferroptosis in RGCs death. Specifically, we show that H_2S regulates iron metabolism, chelates excess iron, restores GPX4 expression, and reduces oxidative stress, highlighting its potential to counteract pressure-induced ferroptosis in the retina. Additionally, we identify NOX2 as an upstream regulator of GPX4, linking NOX2 inhibition to the reduction of ferroptosis. These findings emphasize the multifaceted mechanisms underlying glaucoma and the significance of targeting multiple pathways for effective neuroprotection. In conclusion, the slow-releasing H_2S donor GYY4137 holds promising therapeutic potential for protecting RGCs in glaucoma.

4. Method

4.1. Animal

This study utilized 8–10 week-old male C57BL/6 J wild-type mice ($n = 54$), mtDNA mutator mice aged 37 weeks ($n = 3$), and NOX−/− mice aged 8–9 weeks (n = 3).Both mtDNA mutator mice and $NOX^{-/-}$ mice are on a C57BL/6 J background [65,66]. Prof. Aleksandra Trifunovic generously provided mtDNA mutator mice. $NOX^{-/-}$ mice were kindly provided by Dr. Marc Herb.

MtDNA mutator mice are knock-in mice engineered to express a *Polg* variant that lacks proofreading ability [67]. *Polg* encodes polymerase gamma, the only mitochondrial DNA polymerase involved in all synthetic and repair reactions of mtDNA [65]. Due to effective prevention of proofreading in mtDNA mutator mice, they exhibit an mtDNA mutator phenotype, characterized by a three to fivefold rise in point mutation rates [67].

All animals were housed in pathogen-free, individually ventilated cages (GM 500, Tecniplast® Greenline) at the University of Cologne Medical School's Animal Institute. Food and water were available freely throughout a 12-h light and dark cycle. All animal experiments complied with the German Animal Welfare Act, the EU Directive 2010/63/EU, and the ARVO Declaration. The experiments were evaluated and authorized by the competent authority for animal welfare in North Rhine-Westphalia, Germany (Landesamt für Natur, Umwelt und Verbraucherschutz Nordrhein-Westfalen; approval nos. 4.21.003 and 2020.

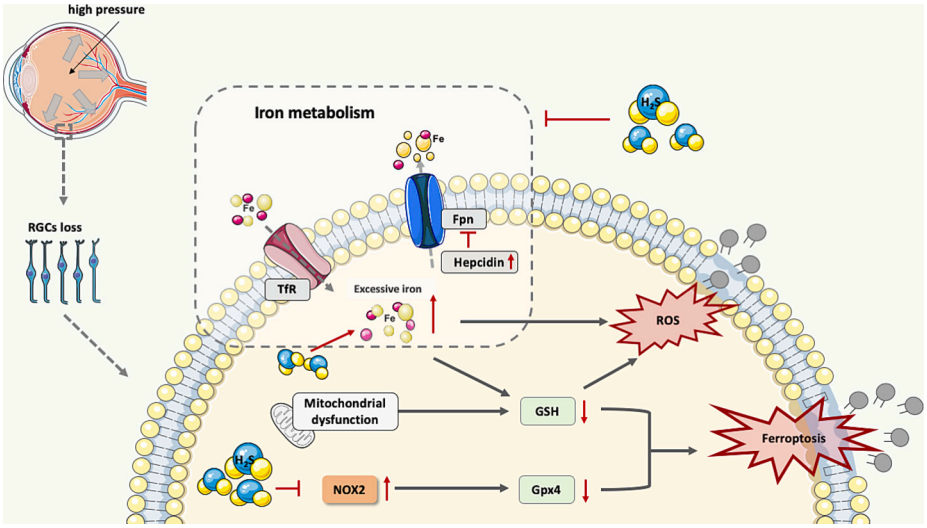

Fig. 7. The schematic representation of the mechanisms underlying high pressure induced RGCs loss and the multifaceted mode of action of H_2S.

A490). All procedures prioritized animal well-being, adhered to ethical guidelines, and minimized suffering in strict accordance with current legislation.

4.2. Subacute IOP elevation animal model in vivo

Episcleral vein occlusion (EVO) is a commonly used method to induce subacute IOP elevation, characterized by a gradual and sustained increase in IOP over several days to weeks. In this study, IOP is elevated for 14 days, which does not strictly correspond to the definitions of acute or chronic elevation. Referring to this intermediate duration, we define it as "subacute IOP elevation." This model effectively mimics the early stages of glaucoma, allowing for the investigation of pressure-induced RGCs injury and neurodegeneration [21,68]. In this study, EVO was used to induce subacute IOP elevation in wildtype C57BL/6 J mice. Mice were anesthetized with an intraperitoneal injection of ketamine (100 mg/kg) and xylazine (10 mg/kg). Topical anesthesia was applied to the ocular surface using 0.4 % proparacaine hydrochloride eye drops (OmniVision GmbH, Germany). Under a surgical microscope, the conjunctiva and Tenon's capsule were incised along the limbus, followed by two relaxing cuts. The superior and lateral rectus muscles were retracted to expose the episcleral veins. After tissue dissection, fine microforceps were placed beneath the episcleral vein. A handheld thermal cautery unit (Fine Science Tools GmbH, Germany) was used to apply pulsed heat through the microforceps until the vein showed visible congestion, indicating successful occlusion. Ofloxacin ointment was applied afterward to prevent inflammation. The left eye underwent the occlusion procedure, while the right eye served as a control without intervention. Retinas were harvested on post-operative day 14.

IOP was measured with a TonoLab rebound tonometer (iCare, Finland) before surgery and every two days after surgery. Each IOP value was averaged from 10 consecutive measurements. Mice without elevated IOP or with postoperative complications were excluded. IOP data are provided in Supplementary Data S2 ("IOP Changes"). Retinas were harvested on post-operative day 14.

4.3. Preparation of retinal explants

Mice were euthanized using CO_2 asphyxiation. The eye was swiftly excised and placed in a petri dish with cold phosphate buffer saline (PBS, Gibco, Thermo Fisher, MA, USA, pH 7.4). The anterior eye segment was excised, and the retina was meticulously separated from the posterior segment. The retina was then divided into four equal sections and placed flat on filters (Millipore filter, Millicell, Cork, Ireland) with the ganglion cells oriented upwards. The vitreous attached to the retinal surface was then cleaned with flat forceps.

4.4. Protein preparation from retina

Retinas were homogenized with the T-PER tissue protein extraction reagent (REF78510, Thermo Scientific, USA) supplemented with protease inhibitors (P8340, Sigma, USA), and then centrifuged at 10,000 $\times g$ for 5 min. The protein concentration of the supernatant was measured using a BCA assay (WG327090, Thermo Scientific, USA). Proteomic samples were subsequently processed according to the SP3 protocol [69].

4.5. Mass spectrometry and bioinformatics

Samples were assessed in a randomized sequence at the CECAD/CMMC Proteomics Core Facility. The LC-MS system used an Orbitrap Exploris 480 mass spectrometer (Thermo Scientific) coupled with a FAIMSpro differential ion mobility device. This setup was connected to an UltiMate 3000 system (Thermo Scientific, Bremen, Germany). For comprehensive details on sample preparation and instrument parameters, refer to Supplementary Data S1, "Mass Spectrometry Sample Preparation". Raw data were analyzed using Proteome Discoverer 2.0 (Thermo Scientific, Bremen, Germany) and compared to the reviewed *Mus musculus* proteome (UniProt UP000000589), FDR thresholds of 0.01 and 0.05 were applied for strict and moderate criteria, respectively, for both peptides and peptide-spectrum matches. For more specific parameter settings, refer to the previous study [70]. Additional data were analyzed through the online tools PANTHER and STRING [71,72].

4.6. Hydrostatic pressure model in vitro

An in vitro hydrostatic pressure model was employed to explore iron toxicity to retinal neurons and the underlying mechanism of RGCs death under pressure. Retinal explants from wild-type mice and NOX−/− mice were prepared according to the methods described above and were randomly placed into tissue culture dishes (Lumox dish 35, Sarstedt, Germany) for ex vivo culture. The culture medium comprised DMEM/F12 (Dulbecco's Modified Eagle's Medium/Nutrient Mixture F-12; Gibco BRL, Eggenstein, Germany) with 10 μg/mL porcine insulin and 1 % penicillin and streptomycin. The cultures were maintained at 37 °C in an atmosphere containing 5 % CO_2. Retinas were harvested after 24 h of culturing.

4.6.1. Culture treatment

To investigate the effects of iron toxicity on the retina, the iron overload group was cultured in 500 nM Hemin for 1 h and then changed to regular culture medium for another 23 h. Hemin, a heme analog derived from heme (a component of hemoglobin), is an organic form of iron that can be uptaken by mammalian tissues. It has been shown to induce iron overload, and its neurotoxic effects make it a valuable tool for studying the role of iron accumulation in neurodegenerative diseases. Hemin (Fe3+ protoporphyrin IX chloride; 51,280, Sigma-Aldrich, Germany) has been used in in vitro research to simulate iron overload environments due to its slowly releasing ferric iron properties [73,74]. It was dissolved in the culture medium at a concentration of 500 nM. (The concentration was determined by the pilot experiments, see Supplementary Data S3 "Hemin toxicity on RGCs".)

To investigate the effects of subacute pressure elevation on the retina, the high-pressure group was under fluctuating hydrostatic pressure within a pressure incubation chamber for 6 h and in the regular condition at 0 mmHg for the rest of 18 h. During the 6-h culture period, the chamber pressure was initially raised to 60 mmHg and subsequently reduced to 0 mmHg in a 15-min cycle.

The metallic incubation chamber is described in detail in our previous study [21]. GYY4137 is an H_2S precursor with the pharmacological advantage that it releases H_2S slowly and continuously [75]. It has been investigated for its potential therapeutic effects in various diseases, including neurodegenerative conditions and cardiovascular diseases. The H_2S group was cultured under fluctuating pressure with additional 100 nM GYY4137 (Sigma-Aldrich, Darmstadt, Germany).

4.7. Quantification of RGCs

Explants were fixed in 4 % paraformaldehyde (PFA, Carl Roth, Karlsruhe, Germany), cryoprotected in 30 % sucrose solution, and flash-frozen in liquid nitrogen (DE10100211, Linde GmbH Gases Division Pullach) for 10 s. Blocking was performed at room temperature for 1 h using Blotto solution (1 % skim milk and 0.3 % Triton X-100 in PBS). This was followed by overnight incubation at 4°Cwith the anti-Brn3a antibody (1:200; MAB1585, EMD Millipore Corporation, Temecula, CA, USA), diluted in the same Blotto solution. Post-washing with PBS-T, the samples were then exposed to a secondary antibody (1:1000; ab150113, Abcam, Cambridge, UK) for 1 h at room temperature. Fluorescence images of the retina were captured using a fluorescence microscope (Axio Imager M2, ApoTome2, Zeiss) at 20-fold magnification. Images were acquired from six predefined regions of the retina—two areas each from the central, mid-peripheral, and peripheral zones in

each quadrant—to ensure representative sampling across the retina. To maintain consistency, all images were analyzed under identical thresholds and settings to minimize variability. Total numbers of the RGCs were counted using ImageJ software (Fiji v_1), total = 6 counts/quadrant, an average value was calculated and then extrapolated to RGCs/mm2, the mean values were compared between groups. The final results were expressed as the number of Brn3a-positive cells per square millimeter (cells/mm^2).

4.8. Immunofluorescence of iron regulatory proteins

Fixed retinal explants were placed in molds filled with optimal cutting temperature (OCT) compound (Sakura Finetek, California, USA) and frozen on dry ice. The 12-μm thick retinal cryo-sections were made by a cryostat (CM3050S, Leica, Wetzlar, Germany) and air-dried. Retinal cryo-sections were permeabilized and blocked with a blocking solution containing 1 % bovine serum albumin and 0.1 % Triton X-100 for 30 min. Subsequently, the sections were incubated with primary antibodies targeting transferrin receptor (1:200, ab84036, Abcam), hepcidin (1:200, ab190775, Abcam), ferritin light chain (1:200, ab69090, Abcam), and ferritin heavy chain (1:200, ab75973, Abcam) for 2 h. Sections were incubated with a secondary antibody (1:1000, A11010, Life Technologies, Carlsbad, USA) for 1 h in the dark at room temperature. DAPI containing mounting media (BIOZOL Diagnostica Vertrieb GmbH, Eching, Germany) was used for mounting the slices. A confocal fluorescence microscope (Airy Scan confocal, Zeiss) was used to scan the complete retinal tissue at 20-fold magnification. 20 layer-scanned photographs were selected at the same interval and stacked by the *Z*-stack function. The fluorescence intensity was measured by ImageJ in the stacked image.

4.9. Iron quantification

Iron content and composition in the retina and brain were quantified using an iron assay kit (MAK025, Sigma) following the provided instructions. A spectrophotometric multi-well plate reader (TECAN infinite F200 Pro) measured the absorbance at 593 nm.

4.10. Western blotting

Western blotting protocol followed previously established methods [45]. Briefly, retinal tissue was lysed as previously described and sample protein concentrations were determined. Samples containing 20 μg of protein were boiled at 95 °Cfor 5 min. Proteins in the tissues were separated via sodium dodecyl sulfate-polyacrylamide gel electrophoresis (Novex NuPAGE, Thermo Fisher, USA) at 130 V and transferred onto polyvinylidene difluoride membranes (Bio-Rad, Gladesville, Australia). Membranes were washed with PBS-T and blocked with 5 % skimmed milk. After washing the membranes again they were incubated overnight at 4 °C with anti-GPX4 antibody (1:1000, ab125066, Abcam, Cambridge, UK), anti-NOX2 antibody (1:1000, ab129068, Abcam) and anti-beta-actin antibody (1:4000, ab6276, Abcam). Following washes, the membrane was incubated for 1 h with appropriate horseradish peroxidase-conjugated secondary antibodies (1:4000; Sigma-Aldrich). An automated chemiluminescence detection system (Millipore, Billerica, MA, USA) was utilized to detect protein bands. ImageJ software served for quantification.

4.11. Quantification of oxidative stress

GSH is an essential biochemical indicator of oxidative stress levels [76]. The GSH assay kit (ab239727, Abcam) was administered to quantify GSH levels. The fluorescent dye dihydroethidium (DHE) was used to locate and indirectly measure ROS levels. Retinal cryo-sections were stained with DHE (1 μM) as previously described [77]. Photographs were taken with a confocal fluorescence microscope (Airy Scan confocal, Zeiss) at 20-fold magnification and stacked. The fluorescence intensity of DHE was quantified with ImageJ.

4.12. Statistical analysis

The data extraction and analysis were conducted in a blinded manner to ensure objectivity. GraphPad Prism (version 9.2, San Diego, California USA) was used for statistical analysis and graphical presentation. All data are shown as mean ± standard deviation (SD). Two-group comparisons were examined by *t*-test. Multiple comparisons were conducted using one-way analysis of variance (ANOVA) followed by Tukey's post hoc test. Statistical significance was defined as a *p*-value of <0.05.

CRediT authorship contribution statement

Yuan Feng: Writing – original draft, Software, Project administration, Methodology, Investigation, Formal analysis, Data curation. **Xiaosha Wang:** Investigation, Data curation. **Panpan Li:** Formal analysis, Data curation. **Xin Shi:** Formal analysis, Data curation. **Verena Prokosch:** Writing – review & editing, Supervision, Resources, Project administration, Investigation, Funding acquisition, Conceptualization. **Hanhan Liu:** Writing – review & editing, Validation, Supervision, Project administration, Methodology, Investigation, Funding acquisition, Formal analysis, Conceptualization.

Funding statement

This work was supported by German Research Foundation (Deutsche Forschungsgemeinschaft, DFG) with grant PR1569/1-1 and SFB1607 C01, Cologne Clinician Scientist Program.

Declaration of competing interest

The authors declare no conflict of interest.

Acknowledgments

We are very grateful to Prof. Aleksandra Trifunovic and her team for providing us with mtDNA mutator mice. We are also very grateful to Dr. Marc Herb for providing the $NOX^{-/-}$ mice. We also thank Ms. Rodica Maniu for her experimental technical support. We are grateful for the financial support scholarships from the China Scholarship Council.

Appendix A. Supplementary data

Supplementary data to this article can be found online at https://doi.org/10.1016/j.bbadis.2025.167705.

Data availability

The proteomics data supporting the findings of this study have been deposited in ProteomeXchange with the identifier PXD049992. https://www.ebi.ac.uk/pride/profile/reviewer_pxd049992

References

[1] J.B. Jonas, T. Aung, R.R. Bourne, A.M. Bron, R. Ritch, S. Panda-Jonas, Glaucoma, Lancet 390 (10108) (2017) 2183–2193.
[2] L.P. Cohen, L.R. Pasquale, Clinical characteristics and current treatment of glaucoma, Cold Spring Harb. Perspect. Med. 4 (6) (2014).
[3] J. Qu, D. Wang, C.L. Grosskreutz, Mechanisms of retinal ganglion cell injury and defense in glaucoma, Exp. Eye Res. 91 (1) (2010) 48–53.
[4] P. Joshi, A. Dangwal, I. Guleria, S. Kothari, P. Singh, J.M. Kalra, V. Jakhmola, Glaucoma in adults-diagnosis, management, and prediagnosis to end-stage, categorizing glaucoma's stages: a review, J Curr Glaucoma Pract 16 (3) (2022) 170–178.

[5] A. Pascale, F. Drago, S. Govoni, Protecting the retinal neurons from glaucoma: lowering ocular pressure is not enough, Pharmacol. Res. 66 (1) (2012) 19–32.
[6] R. Susanna Jr., C.G. De Moraes, G.A. Cioffi, R. Ritch, Why do people (still) go blind from glaucoma? Transl. Vis. Sci. Technol. 4 (2) (2015) 1.
[7] Y.H. Kwon, C.S. Kim, M.B. Zimmerman, W.L. Alward, S.S. Hayreh, Rate of visual field loss and long-term visual outcome in primary open-angle glaucoma, Am. J. Ophthalmol. 132 (1) (2001) 47–56.
[8] P.R. Lichter, Glaucoma clinical trials and what they mean for our patients, Am. J. Ophthalmol. 136 (1) (2003) 136–145.
[9] R. Tabassum, N.Y. Jeong, J. Jung, Therapeutic importance of hydrogen sulfide in age-associated neurodegenerative diseases, Neural Regen. Res. 15 (4) (2020) 653–662.
[10] F.N. Salloum, Hydrogen sulfide and cardioprotection–mechanistic insights and clinical translatability, Pharmacol. Ther. 152 (2015) 11–17.
[11] S. Panthi, H.J. Chung, J. Jung, N.Y. Jeong, Physiological importance of hydrogen sulfide: emerging potent neuroprotector and neuromodulator, Oxid. Med. Cell. Longev. 2016 (2016) 9049782.
[12] S. Huang, P. Huang, H. Yu, Z. Lin, X. Liu, X. Shen, L. Guo, Y. Zhong, Extracellular signal-regulated kinase 1/2 pathway is insufficiently involved in the neuroprotective effect by hydrogen sulfide supplement in experimental glaucoma, Invest. Ophthalmol. Vis. Sci. 60 (13) (2019) 4346–4359.
[13] Y. Feng, V. Prokosch, H. Liu, Current perspective of hydrogen sulfide as a novel gaseous modulator of oxidative stress in glaucoma, Antioxidants (Basel) 10 (5) (2021).
[14] Y. Liu, Y. Deng, H. Liu, C. Yin, X. Li, Q. Gong, Corrigendum to: "Hydrogen sulfide ameliorates learning memory impairment in APP/PS1 transgenic mice: A novel mechanism mediated by the activation of Nrf2" [Pharmacol. Biochem. Behav. 150-151 (2016) 207-216], Pharmacology, Biochemistry, and Behavior 153 (2017) 191.
[15] Y. Liu, Y. Deng, H. Liu, C. Yin, X. Li, Q. Gong, Hydrogen sulfide ameliorates learning memory impairment in APP/PS1 transgenic mice: a novel mechanism mediated by the activation of Nrf2, Pharmacol. Biochem. Behav. 150-151 (2016) 207–216.
[16] L. Xie, S. Yu, K. Yang, C. Li, Y. Liang, Hydrogen sulfide inhibits Autophagic neuronal cell death by reducing oxidative stress in spinal cord ischemia reperfusion injury, Oxid. Med. Cell. Longev. 2017 (2017) 8640284.
[17] M.R. Sarookhani, H. Haghdoost-Yazdi, A. Sarbazi-Golezari, A. Babayan-Tazehkand, N. Rastgoo, Involvement of adenosine triphosphate-sensitive potassium channels in the neuroprotective activity of hydrogen sulfide in the 6-hydroxydopamine-induced animal model of Parkinson's disease, Behav. Pharmacol. 29 (4) (2018) 336–343.
[18] K. Sakamoto, Y. Suzuki, Y. Kurauchi, A. Mori, T. Nakahara, K. Ishii, Hydrogen sulfide attenuates NMDA-induced neuronal injury via its anti-oxidative activity in the rat retina, Exp. Eye Res. 120 (2014) 90–96.
[19] J. Biermann, W.A. Lagreze, N. Schallner, C.I. Schwer, U. Goebel, Inhalative preconditioning with hydrogen sulfide attenuated apoptosis after retinal ischemia/reperfusion injury, Mol. Vis. 17 (2011) 1275–1286.
[20] Y.F. Si, J. Wang, J. Guan, L. Zhou, Y. Sheng, J. Zhao, Treatment with hydrogen sulfide alleviates streptozotocin-induced diabetic retinopathy in rats, Br. J. Pharmacol. 169 (3) (2013) 619–631.
[21] H. Liu, F. Anders, S. Thanos, C. Mann, A. Liu, F.H. Grus, N. Pfeiffer, V. Prokosch-Willing, Hydrogen sulfide protects retinal ganglion cells against glaucomatous injury in vitro and in vivo, Invest. Ophthalmol. Vis. Sci. 58 (12) (2017) 5129–5141.
[22] G. Yang, L. Wu, B. Jiang, W. Yang, J. Qi, K. Cao, Q. Meng, A.K. Mustafa, W. Mu, S. Zhang, S.H. Snyder, R. Wang, H2S as a physiologic vasorelaxant: hypertension in mice with deletion of cystathionine gamma-lyase, Science 322 (5901) (2008) 587–590.
[23] Y. Kaneko, Y. Kimura, H. Kimura, I. Niki, L-cysteine inhibits insulin release from the pancreatic beta-cell: possible involvement of metabolic production of hydrogen sulfide, a novel gasotransmitter, Diabetes 55 (5) (2006) 1391–1397.
[24] H. Zhang, M. Bhatia, Hydrogen sulfide: a novel mediator of leukocyte activation, Immunopharmacol. Immunotoxicol. 30 (4) (2008) 631–645.
[25] H. Liu, N. Perumal, C. Manicam, K. Mercieca, V. Prokosch, Proteomics reveals the potential protective mechanism of hydrogen sulfide on retinal ganglion cells in an ischemia/reperfusion injury animal model, Pharmaceuticals (Basel) 13 (9) (2020).
[26] F. Yao, J. Peng, E. Zhang, D. Ji, Z. Gao, Y. Tang, X. Yao, X. Xia, Pathologically high intraocular pressure disturbs normal iron homeostasis and leads to retinal ganglion cell ferroptosis in glaucoma, Cell Death Differ. 30 (1) (2023) 69–81.
[27] S. Dutt, I. Hamza, T.B. Bartnikas, Molecular mechanisms of Iron and Heme metabolism, Annu. Rev. Nutr. 42 (2022) 311–335.
[28] A. Ashok, N. Singh, S. Chaudhary, V. Bellamkonda, A.E. Kritikos, A.S. Wise, N. Rana, D. McDonald, R. Ayyagari, Retinal degeneration and Alzheimer's disease: an evolving link, Int. J. Mol. Sci. 21 (19) (2020).
[29] W.D. Ramdas, The relation between dietary intake and glaucoma: a systematic review, Acta Ophthalmol. 96 (6) (2018) 550–556.
[30] S.Y. Wang, K. Singh, S.C. Lin, The association between glaucoma prevalence and supplementation with the oxidants calcium and iron, Invest. Ophthalmol. Vis. Sci. 53 (2) (2012) 725–731.
[31] F. Yao, J. Peng, E. Zhang, D. Ji, Z. Gao, Y. Tang, X. Yao, X. Xia, Pathologically high intraocular pressure disturbs normal iron homeostasis and leads to retinal ganglion cell ferroptosis in glaucoma, Cell Death Differ. (2022).
[32] A. Ashraf, J. Jeandriens, H.G. Parkes, P.W. So, Iron dyshomeostasis, lipid peroxidation and perturbed expression of cystine/glutamate antiporter in Alzheimer's disease: evidence of ferroptosis, Redox Biol. 32 (2020) 101494.
[33] A.A. Belaidi, A.I. Bush, Iron neurochemistry in Alzheimer's disease and Parkinson's disease: targets for therapeutics, J. Neurochem. 139 (Suppl. 1) (2016) 179–197.
[34] D.H. Mahad, B.D. Trapp, H. Lassmann, Pathological mechanisms in progressive multiple sclerosis, Lancet Neurol. 14 (2) (2015) 183–193.
[35] J. Li, F. Cao, H.L. Yin, Z.J. Huang, Z.T. Lin, N. Mao, B. Sun, G. Wang, Ferroptosis: past, present and future, Cell Death Dis. 11 (2) (2020) 88.
[36] S.J. Dixon, K.M. Lemberg, M.R. Lamprecht, R. Skouta, E.M. Zaitsev, C.E. Gleason, D.N. Patel, A.J. Bauer, A.M. Cantley, W.S. Yang, B. Morrison 3rd, B.R. Stockwell, Ferroptosis: an iron-dependent form of nonapoptotic cell death, Cell 149 (5) (2012) 1060–1072.
[37] P. Aisen, C. Enns, M. Wessling-Resnick, Chemistry and biology of eukaryotic iron metabolism, Int. J. Biochem. Cell Biol. 33 (10) (2001) 940–959.
[38] M. Yang, K.F. So, W.C. Lam, A.C. Yin Lo, Ferroptosis and glaucoma: implications in retinal ganglion cell damage and optic nerve survival, Neural Regen. Res. 18 (3) (2023) 545–546.
[39] H.M. Arif, Z. Qian, R. Wang, Signaling integration of hydrogen sulfide and Iron on cellular functions, Antioxid. Redox Signal. 36 (4–6) (2022) 275–293.
[40] J.P. Gnana-Prakasam, P.M. Martin, S.B. Smith, V. Ganapathy, Expression and function of iron-regulatory proteins in retina, IUBMB Life 62 (5) (2010) 363–370.
[41] J.P. Gnana-Prakasam, P.M. Martin, B.A. Mysona, P. Roon, S.B. Smith, V. Ganapathy, Hepcidin expression in mouse retina and its regulation via lipopolysaccharide/toll-like receptor-4 pathway independent of Hfe, Biochem. J. 411 (1) (2008) 79–88.
[42] N. Kajarabille, G.O. Latunde-Dada, Programmed cell-death by ferroptosis: antioxidants as mitigators, Int. J. Mol. Sci. 20 (19) (2019).
[43] G.Y. Lam, J. Huang, J.H. Brumell, The many roles of NOX2 NADPH oxidase-derived ROS in immunity, Semin. Immunopathol. 32 (4) (2010) 415–430.
[44] W.S. Yang, R. SriRamaratnam, M.E. Welsch, K. Shimada, R. Skouta, V. S. Viswanathan, J.H. Cheah, P.A. Clemons, A.F. Shamji, C.B. Clish, L.M. Brown, A. W. Girotti, V.W. Cornish, S.L. Schreiber, B.R. Stockwell, Regulation of ferroptotic cancer cell death by GPX4, Cell 156 (1–2) (2014) 317–331.
[45] X. Shi, P. Li, M. Herb, H. Liu, M. Wang, X. Wang, Y. Feng, T. van Beers, N. Xia, H. Li, V. Prokosch, Pathological high intraocular pressure induces glial cell reactive proliferation contributing to neuroinflammation of the blood-retinal barrier via the NOX2/ET-1 axis-controlled ERK1/2 pathway, J. Neuroinflammation 21 (1) (2024) 105.
[46] J. Zhu, H. Chen, J. Wu, S. Li, W. Lin, N. Wang, L. Bai, Ferroptosis in glaucoma: a promising avenue for therapy, Adv Biol (Weinh) 8 (5) (2024) e2300530.
[47] S. Huang, K. Liu, Y. Su, F. Wang, T. Feng, Research progress of ferroptosis in glaucoma and optic nerve damage, Mol. Cell. Biochem. 478 (4) (2023) 721–727.
[48] M.W. Park, H.W. Cha, J. Kim, J.H. Kim, H. Yang, S. Yoon, N. Boonpraman, S.S. Yi, I.D. Yoo, J.S. Moon, NOX4 promotes ferroptosis of astrocytes by oxidative stress-induced lipid peroxidation via the impairment of mitochondrial metabolism in Alzheimer's diseases, Redox Biol. 41 (2021) 101947.
[49] Y. Maimaiti, T. Su, Z. Zhang, L. Ma, Y. Zhang, H. Xu, NOX4-mediated astrocyte ferroptosis in Alzheimer's disease, Cell Biosci. 14 (1) (2024) 88.
[50] X. Liu, X. Liu, Y. Wang, H. Sun, Z. Guo, X. Tang, J. Li, X. Xiao, S. Zheng, M. Yu, C. He, J. Xu, W. Sun, Proteome characterization of Glaucoma aqueous humor, Mol. Cell. Proteomics 20 (2021) 100117.
[51] C. Camaschella, A. Nai, L. Silvestri, Iron metabolism and iron disorders revisited in the hepcidin era, Haematologica 105 (2) (2020) 260–272.
[52] F. Petit, A. Drecourt, M. Dussiot, C. Zangarelli, O. Hermine, A. Munnich, A. Rotig, Defective palmitoylation of transferrin receptor triggers iron overload in Friedreich ataxia fibroblasts, Blood 137 (15) (2021) 2090–2102.
[53] M. Theurl, D. Song, E. Clark, J. Sterling, S. Grieco, S. Altamura, B. Galy, M. Hentze, M.U. Muckenthaler, J.L. Dunaief, Mice with hepcidin-resistant ferroportin accumulate iron in the retina, FASEB J. 30 (2) (2016) 813–823.
[54] B.B. Muhoberac, R. Vidal, Iron, ferritin, hereditary ferritinopathy, and neurodegeneration, Front. Neurosci. 13 (2019) 1195.
[55] S. Masaldan, A.I. Bush, D. Devos, A.S. Rolland, C. Moreau, Striking while the iron is hot: iron metabolism and ferroptosis in neurodegeneration, Free Radic. Biol. Med. 133 (2019) 221–233.
[56] A. Ayala, M.F. Munoz, S. Arguelles, Lipid peroxidation: production, metabolism, and signaling mechanisms of malondialdehyde and 4-hydroxy-2-nonenal, Oxid. Med. Cell. Longev. 2014 (2014) 360438.
[57] M.M. Gaschler, A.A. Andia, H. Liu, J.M. Csuka, B. Hurlocker, C.A. Vaiana, D. W. Heindel, D.S. Zuckerman, P.H. Bos, E. Reznik, L.F. Ye, Y.Y. Tyurina, A.J. Lin, M. S. Shchepinov, A.Y. Chan, E. Peguero-Pereira, M.A. Fomich, J.D. Daniels, A. V. Bekish, V.V. Shmanai, V.E. Kagan, L.K. Mahal, K.A. Woerpel, B.R. Stockwell, FINO(2) initiates ferroptosis through GPX4 inactivation and iron oxidation, Nat. Chem. Biol. 14 (5) (2018) 507–515.
[58] T. Ma, J. Du, Y. Zhang, Y. Wang, B. Wang, T. Zhang, GPX4-independent ferroptosis-a new strategy in disease's therapy, Cell Death Discov 8 (1) (2022) 434.
[59] F. Ursini, M. Maiorino, Lipid peroxidation and ferroptosis: the role of GSH and GPx4, Free Radic. Biol. Med. 152 (2020) 175–185.
[60] S.J. Dixon, B.R. Stockwell, The role of iron and reactive oxygen species in cell death, Nat. Chem. Biol. 10 (1) (2014) 9–17.
[61] G.J. Kontoghiorghes, C.N. Kontoghiorghe, Iron and chelation in biochemistry and medicine: new approaches to controlling iron metabolism and treating related diseases, Cells 9 (6) (2020).
[62] A.D. Read, R.E. Bentley, S.L. Archer, K.J. Dunham-Snary, Mitochondrial iron-sulfur clusters: structure, function, and an emerging role in vascular biology, Redox Biol. 47 (2021) 102164.
[63] R. Wang, Two's company, three's a crowd: can H2S be the third endogenous gaseous transmitter? FASEB J. 16 (13) (2002) 1792–1798.
[64] M. Eberhardt, M. Dux, B. Namer, J. Miljkovic, N. Cordasic, C. Will, T.I. Kichko, J. de la Roche, M. Fischer, S.A. Suarez, D. Bikiel, K. Dorsch, A. Leffler, A. Babes, A. Lampert, J.K. Lennerz, J. Jacobi, M.A. Marti, F. Doctorovich, E.D. Hogestatt, P.

M. Zygmunt, I. Ivanovic-Burmazovic, K. Messlinger, P. Reeh, M.R. Filipovic, H2S and NO cooperatively regulate vascular tone by activating a neuroendocrine HNO-TRPA1-CGRP signalling pathway, Nat. Commun. 5 (2014) 4381.
[65] N. Hance, M.I. Ekstrand, A. Trifunovic, Mitochondrial DNA polymerase gamma is essential for mammalian embryogenesis, Hum. Mol. Genet. 14 (13) (2005) 1775–1783.
[66] J.D. Pollock, D.A. Williams, M.A. Gifford, L.L. Li, X. Du, J. Fisherman, S.H. Orkin, C.M. Doerschuk, M.C. Dinauer, Mouse model of X-linked chronic granulomatous disease, an inherited defect in phagocyte superoxide production, Nat. Genet. 9 (2) (1995) 202–209.
[67] A. Trifunovic, A. Wredenberg, M. Falkenberg, J.N. Spelbrink, A.T. Rovio, C. E. Bruder, Y.M. Bohlooly, S. Gidlof, A. Oldfors, R. Wibom, J. Tornell, H.T. Jacobs, N.G. Larsson, Premature ageing in mice expressing defective mitochondrial DNA polymerase, Nature 429 (6990) (2004) 417–423.
[68] M. Wang, H. Liu, N. Xia, H. Li, T. van Beers, A. Gericke, V. Prokosch, Intraocular pressure-induced endothelial dysfunction of retinal blood vessels is persistent, but does not trigger retinal ganglion cell loss, Antioxidants (Basel) 11 (10) (2022).
[69] C.S. Hughes, S. Moggridge, T. Muller, P.H. Sorensen, G.B. Morin, J. Krijgsveld, Single-pot, solid-phase-enhanced sample preparation for proteomics experiments, Nat. Protoc. 14 (1) (2019) 68–85.
[70] S. Bekeschus, J.W. Lackmann, D. Gumbel, M. Napp, A. Schmidt, K. Wende, A neutrophil proteomic signature in surgical trauma wounds, Int. J. Mol. Sci. 19 (3) (2018).
[71] P.D. Thomas, D. Ebert, A. Muruganujan, T. Mushayahama, L.P. Albou, H. Mi, PANTHER: making genome-scale phylogenetics accessible to all, Protein Sci. 31 (1) (2022) 8–22.
[72] D. Szklarczyk, R. Kirsch, M. Koutrouli, K. Nastou, F. Mehryary, R. Hachilif, A. L. Gable, T. Fang, N.T. Doncheva, S. Pyysalo, P. Bork, L.J. Jensen, C. von Mering, The STRING database in 2023: protein-protein association networks and functional enrichment analyses for any sequenced genome of interest, Nucleic Acids Res. 51 (D1) (2023) D638–D646.
[73] N. Seiwert, S. Wecklein, P. Demuth, S. Hasselwander, T.A. Kemper, T. Schwerdtle, T. Brunner, J. Fahrer, Heme oxygenase 1 protects human colonocytes against ROS formation, oxidative DNA damage and cytotoxicity induced by heme iron, but not inorganic iron, Cell Death Dis. 11 (9) (2020) 787.
[74] L.S. Marton, X. Wang, A. Kowalczuk, Z.D. Zhang, E. Windmeyer, R.L. Macdonald, Effects of hemoglobin on heme oxygenase gene expression and viability of cultured smooth muscle cells, Am. J. Physiol. Heart Circ. Physiol. 279 (5) (2000). H2405-13.
[75] D.S. Nin, S.B. Idres, Z.J. Song, P.K. Moore, L.W. Deng, Biological effects of morpholin-4-ium 4 methoxyphenyl (morpholino) phosphinodithioate and other phosphorothioate-based hydrogen sulfide donors, Antioxid. Redox Signal. 32 (2) (2020) 145–158.
[76] G. Noctor, G. Queval, A. Mhamdi, S. Chaouch, C.H. Foyer, Glutathione, Arabidopsis Book vol. 9 (2011) e0142.
[77] A. Gericke, C. Mann, J.K. Zadeh, A. Musayeva, I. Wolff, M. Wang, N. Pfeiffer, A. Daiber, H. Li, N. Xia, V. Prokosch, Elevated intraocular pressure causes abnormal reactivity of mouse retinal arterioles, Oxid. Med. Cell. Longev. 2019 (2019) 9736047.